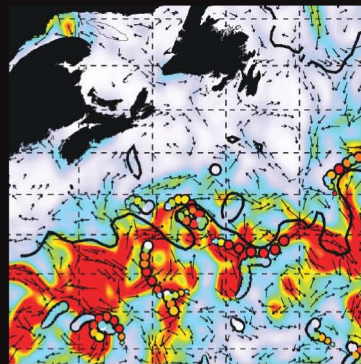
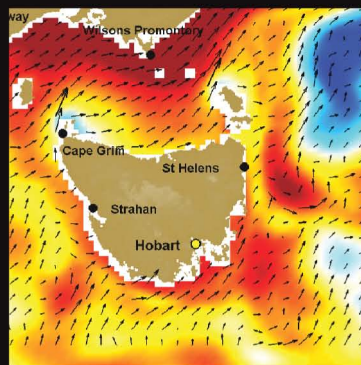
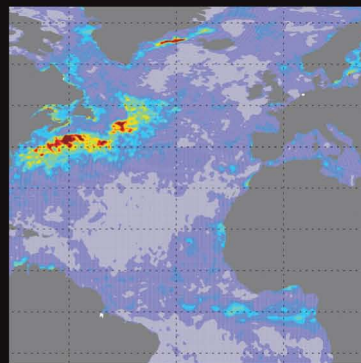
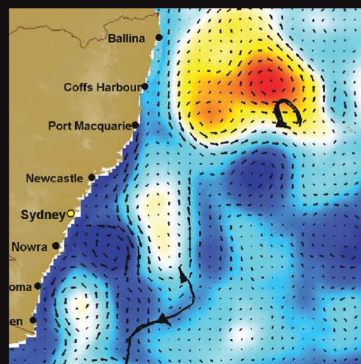
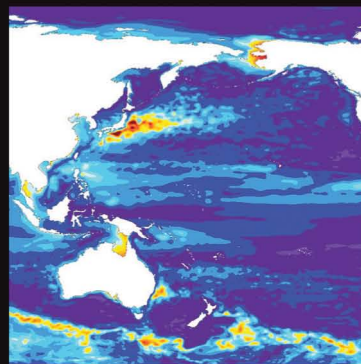


# HIGH-RESOLUTION GLOBAL AND BASIN-SCALE OCEAN ANALYSES AND FORECASTS

BY HARLEY E. HURLBURT, GARY B. BRASSINGTON,  
YANN DRILLET, MASAFUMI KAMACHI, MOUNIR BENKIRAN,  
ROMAIN BOURDALLÉ-BADIE, ERIC P. CHASSIGNET,  
GREGG A. JACOBS, OLIVIER LE GALLOUDEC,  
JEAN-MICHEL LELLOUCHE, E. JOSEPH METZGER,  
PETER R. OKE, TIMOTHY F. PUGH, ANDREAS SCHILLER,  
OLE MARTIN SMEDSTAD, BENOIT TRANCHANT,  
HIROYUKI TSUJINO, NORIHISA USUI, AND ALAN J. WALLCRAFT



Report Documentation Page				Form Approved OMB No. 0704-0188	
Public reporting burden for the collection of information is estimated to average 1 hour per response, including the time for reviewing instructions, searching existing data sources, gathering and maintaining the data needed, and completing and reviewing the collection of information. Send comments regarding this burden estimate or any other aspect of this collection of information, including suggestions for reducing this burden, to Washington Headquarters Services, Directorate for Information Operations and Reports, 1215 Jefferson Davis Highway, Suite 1204, Arlington VA 22202-4302. Respondents should be aware that notwithstanding any other provision of law, no person shall be subject to a penalty for failing to comply with a collection of information if it does not display a currently valid OMB control number.					
1. REPORT DATE <b>2009</b>		2. REPORT TYPE		3. DATES COVERED <b>00-00-2009 to 00-00-2009</b>	
4. TITLE AND SUBTITLE <b>High-Resolution Global and Basin-Scale Ocean Analyses and Forecasts</b>				5a. CONTRACT NUMBER	
				5b. GRANT NUMBER	
				5c. PROGRAM ELEMENT NUMBER	
6. AUTHOR(S)				5d. PROJECT NUMBER	
				5e. TASK NUMBER	
				5f. WORK UNIT NUMBER	
7. PERFORMING ORGANIZATION NAME(S) AND ADDRESS(ES) <b>Naval Research Laboratory, Oceanographic Division, Stennis Space Center, MS, 39529-5004</b>				8. PERFORMING ORGANIZATION REPORT NUMBER	
9. SPONSORING/MONITORING AGENCY NAME(S) AND ADDRESS(ES)				10. SPONSOR/MONITOR'S ACRONYM(S)	
				11. SPONSOR/MONITOR'S REPORT NUMBER(S)	
12. DISTRIBUTION/AVAILABILITY STATEMENT <b>Approved for public release; distribution unlimited</b>					
13. SUPPLEMENTARY NOTES					
14. ABSTRACT					
15. SUBJECT TERMS					
16. SECURITY CLASSIFICATION OF:			17. LIMITATION OF ABSTRACT <b>Same as Report (SAR)</b>	18. NUMBER OF PAGES <b>18</b>	19a. NAME OF RESPONSIBLE PERSON
a. REPORT <b>unclassified</b>	b. ABSTRACT <b>unclassified</b>	c. THIS PAGE <b>unclassified</b>			

**ABSTRACT.** The feasibility of global ocean weather prediction was just emerging as the Global Ocean Data Assimilation Experiment (GODAE) began in 1997. Ocean weather includes phenomena such as meandering currents and fronts, eddies, the surface mixed layer and sea surface temperature (SST), equatorial and coastally trapped waves, upwelling of cold water, and Rossby waves, all influencing ocean variables such as temperature (T), salinity (S), currents, and sea surface height (SSH). Adequate real-time data input, computing power, numerical ocean models, data assimilation capabilities, atmospheric forcing, and bathymetric/boundary constraints are essential to make such prediction possible. The key observing systems and real-time data inputs are SSH from satellite altimetry, satellite and in situ SST, T, or T and S profiles (e.g., Argo, TAO/Triton, PIRATA moored array in the Atlantic, bathythermographs), and atmospheric forcing. The ocean models dynamically interpolate data in conjunction with data assimilation, convert atmospheric forcing into oceanic responses, and forecast the ocean weather, applying bathymetric/boundary constraints in the process. The results are substantially influenced by ocean model simulation skill and it is advantageous to use an ocean model that is eddy-resolving (nominally  $1/10^\circ$  or finer), not just eddy-permitting. Because the most abundant ocean observations are satellite surface data, and subsurface data are very sparse in relation to the spatial scales of the mesoscale ocean features that dominate the ocean interior, downward projection of surface data is a key challenge in ocean data assimilation. The need for accurate prediction of ocean features that are inadequately observed, such as mixed layer depth, places a major burden on the ocean model, data assimilation, and atmospheric forcing. The sensitivity of ocean phenomena to atmospheric forcing and the time scale for response affect the time scale for oceanic predictive skill, sensitivity to the initial state versus the atmospheric forcing as a function of forecast length, and thus oceanic data requirements and prediction system design. Outside of surface boundary layers and shallow regions, forecast skill is about one month globally and over many subregions, and is only modestly reduced by using climatological forcing after the end of atmospheric forecasts versus using analysis-quality forcing for the duration. In addition, global ocean prediction systems must demonstrate the ability to provide initial and boundary conditions to nested regional and coastal models that enhance their predictive skill. Demonstrations of feasibility in relation to the preceding phenomena, requirements, and challenges are drawn from the following global and basin-scale ocean prediction systems: BLUElink> (Australia), the HYbrid Coordinate Ocean Model (HYCOM; USA), Mercator (France), Multivariate Ocean Variational Estimation/Meteorological Research Institute Community Ocean Model (MOVE/MRI.COM; Japan), and the Naval Research Laboratory Layered Ocean Model (NLOM; USA).

## INTRODUCTION

At the beginning of the Global Ocean Data Assimilation Experiment (GODAE) in 1997, the feasibility of global ocean prediction at the mesoscale, about 50–500 km, was considered primarily in terms of enabling technologies, which are discussed in this issue by Clark et al., Roemmich et al., and Dombrowsky et al. At the end of GODAE, we can demonstrate feasibility based on the capabilities and limitations of present real-time operational and pre-operational GODAE ocean prediction systems, discussed here for high-resolution global and basin-scale nowcasts and forecasts at the mesoscale. We also include some indications of the potential for future increases in capability.

Feasibility demonstrations cover the key capabilities needed for global and basin-scale ocean prediction systems. In particular, they must have the ability to nowcast and forecast (1) deep ocean mesoscale variability, including individual eddies and meanders of ocean currents and fronts, (2) sea surface temperature (SST) with accuracy sufficient for user applications and future coupled atmosphere-ocean and Earth system prediction systems, and (3) coastal region phenomena, such as upwelling of cold water and the generation and propagation of coastally trapped waves, with skill sufficient to provide useful results for applications and useful boundary and initial conditions for nested coastal models with higher resolution or added capability,

such as tides. In the next section, we discuss the link between ocean model resolution and ocean dynamics and its implications for nowcasting/forecasting of mesoscale variability. The following two sections present nowcast and forecast demonstrations of mesoscale ocean features with examples of evaluations for individual features. These evaluations can be done routinely in real time or near-real time using independent data not assimilated by the prediction systems. The next two sections

address quantitative forecast evaluation and interpretation of the results, and provide an example where longer range mesoscale forecasting is possible. After that, we demonstrate SST forecast skill superior to persistence (a forecast of no change). So far, persistence of the initial time SST analysis is the approach used in atmospheric forecast models. The final section of this article presents a demonstration of coastal region performance in nowcasting and forecasting of coastally trapped waves.

## NEED FOR AN EDDY-RESOLVING OCEAN MODEL

As noted in the abstract, an eddy-resolving ocean model is one of the components that is essential for ocean prediction at the mesoscale. The simulation skill of the ocean model is critical because of its roles in (1) dynamical interpolation of the data during assimilation, (2) representing the poorly observed subsurface ocean, (3) converting atmospheric forcing into ocean responses, (4) accurately applying topographic/geometric constraints, (5) producing forecasts of “ocean weather,” and (6) providing boundary conditions and initial conditions for nested regional and coastal models with even higher resolution. An eddy-resolving ocean model is also required to resolve the physics of baroclinic instability, which means the model must (a) resolve the first baroclinic Rossby radius of deformation because of its relation to the predominant spatial scale for baroclinic instability, (b) be able to simulate strong, baroclinically unstable inertial jets (and associated recirculation gyres) that penetrate far into the ocean interior, and (c) resolve the physics of baroclinic instability very well in order to transfer sufficient energy into the abyssal layer. The resulting eddy-driven abyssal currents can in turn steer the pathways of upper ocean currents in regions outside the tropics. Thus, baroclinic instability in combination with topographic influences and barotropic instability strongly influence the spatial scales, evolution, amplitude, and propagation of ocean eddies and current/frontal meanders, and in addition, the mean pathways of upper ocean currents. The model resolution required to meet

---

**Harley E. Hurlburt** ([hurlburt@nrlssc.navy.mil](mailto:hurlburt@nrlssc.navy.mil)) is Senior Scientist for Ocean Modeling and Prediction, Oceanography Division, Naval Research Laboratory (NRL), Stennis Space Center, MS, USA. **Gary B. Brassington** is Senior Professional Officer, Ocean Forecasting, Centre for Australian Weather and Climate Research, Bureau of Meteorology (BoM), Melbourne, Australia. **Yann Drillet** is Head, Research and Development Activities, Mercator Océan, Ramonville-Saint-Agne, France. **Masafumi Kamachi** is Head, Second Laboratory, Oceanographic Research Department, Meteorological Research Institute, Tsukuba, Japan. **Mounir Benkiran** is Senior Scientist for Ocean Data Assimilation, CLS Space Oceanography Division, Ramonville-Saint-Agne, France. **Romain Bourdallé-Badie** is Senior Scientist for Physical Ocean Modeling, Centre for Research and Advanced Training in Scientific Computation (CERFACS), Toulouse, France. **Eric P. Chassignet** is Professor and Director, Center for Ocean-Atmospheric Prediction Studies (COAPS), Florida State University, Tallahassee, FL, USA. **Gregg A. Jacobs** is Head, Ocean Dynamics and Prediction Branch, Oceanography Division, NRL, Stennis Space Center, MS, USA. **Olivier Le Galloudec** is Research Engineer for Physical Ocean Modeling, Mercator Océan, Ramonville-Saint-Agne, France. **Jean-Michel Lellouche** is Senior Scientist for Ocean Data Assimilation, Mercator Océan, Ramonville-Saint-Agne, France. **E. Joseph Metzger** is Meteorologist, Oceanography Division, NRL, Stennis Space Center, MS, USA. **Peter R. Oke** is Research Scientist, Centre for Australian Weather and Climate Research, Commonwealth Scientific and Industrial Research Organisation (CSIRO), Hobart, Tasmania, Australia. **Timothy F. Pugh** is Senior IT Officer, Centre for Australian Weather and Climate Research, BoM, Melbourne, Australia. **Andreas Schiller** is Research Scientist, Centre for Australian Weather and Climate Research, CSIRO, Hobart, Tasmania, Australia. **Ole Martin Smedstad** is Principal Scientist, QinetiQ North America, Technology Solutions Group, Stennis Space Center, MS, USA. **Benoit Tranchant** is Senior Scientist for Ocean Data Assimilation, CERFACS, Toulouse, France. **Hiroyuki Tsujino** is Senior Scientist, First Laboratory, Oceanographic Research Department, Meteorological Research Institute, Tsukuba, Japan. **Norihisa Usui** is Scientist, Second Laboratory, Oceanographic Research Department, Meteorological Research Institute, Tsukuba, Japan. **Alan J. Wallcraft** is Computer Scientist, Oceanography Division, NRL, Stennis Space Center, MS, USA.



these criteria varies with location and can range from  $1/10^\circ$  to  $1/25^\circ$  (10 to 3 km for each model variable).

A global or basin-scale model that generates eddies and current meanders but does not adequately meet the preceding criteria is termed eddy-permitting. See Hurlburt et al. (2008a,b) for additional discussion of this topic, and see Emery et al. (1984), Chelton et al. (1998), and Oh et al. (2000) to find observation-based estimates of the first baroclinic Rossby radius of deformation over most of the global ocean. An eddy-permitting model may be adequate where baroclinic instability is not significant, but eddies are ubiquitous over most of the global ocean (Ducet et al., 2000) even where sea surface height (SSH) variability is low (Figure 1a), a situation also demonstrated by eddy-resolving GODAE ocean prediction systems (see Web page list in Dombrowsky et al., 2009). In a nonassimilative basin-scale model, Hurlburt and Hogan (2000) found an explosion of strong eddies over the ocean interior when the ocean model resolution was increased from eddy-permitting (14 km) to eddy-resolving (7 km), while maintaining relatively low SSH variability in the ocean interior in line with satellite altimetry.

Still, a comparison between SSH variability simulated by a model (without ocean data assimilation) and SSH variability measured by satellite altimetry is a useful first step in assessing the ability of the model to represent mesoscale variability. Mesoscale variability is the leading deep-water source of SSH variability retained in the altimetry maps outside the waveguides for equatorial and coastally trapped waves. Thus, one might expect an eddy-resolving model

to simulate higher variability and more realistic patterns of variability than an eddy-permitting model. Figure 1 is a global comparison of SSH variability over 2004–2006 as simulated by (c)  $1/4^\circ$  and (b)  $1/12^\circ$  Mercator without data assimilation and (a) as calculated

from weekly model-independent  $1/12^\circ$  analyses of sea level anomalies from satellite altimetry data (performed at the CLS Space Oceanography Division).

The global pattern and amplitude of the model-simulated variability is quite similar to that from the altimetry, with

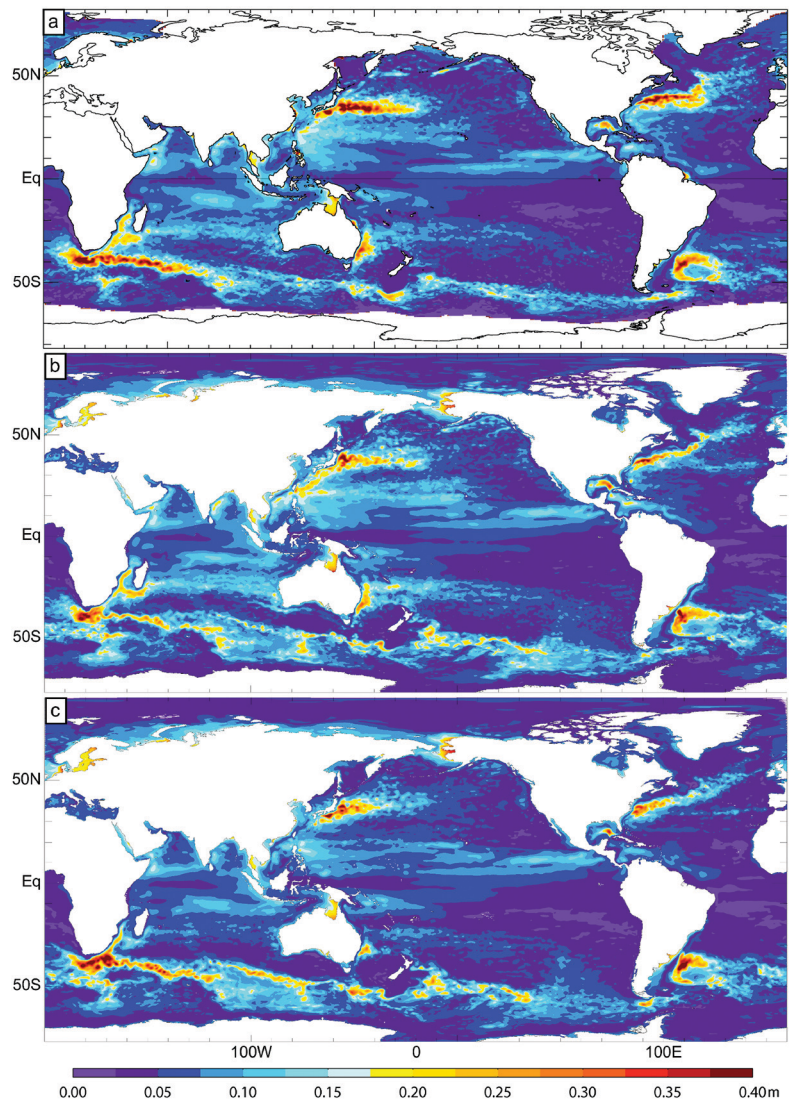


Figure 1. 2004–2006 root mean square (RMS) sea surface height (SSH) variability (m) calculated from (a)  $1/3^\circ$  CLS analyses of altimetry data and (b,c) global Mercator simulations run without ocean data assimilation using (b) the  $1/12^\circ$  ORCA12 and (c) the  $1/4^\circ$  ORCA025 grid configurations. Both have 50 depth-coordinate levels in the vertical, partial cell topography (Barnier et al., 2006), and daily-mean interannual forcing from the European Centre for Medium-Range Weather Forecasts (ECMWF). The global mean RMS SSH over the domain sampled by the altimetry is (a) 7.26 cm for the CLS analyses, (b) 7.51 cm for the  $1/12^\circ$ , and (c) 6.76 cm for the  $1/4^\circ$  Mercator simulations.

an almost one-to-one correspondence between large and small features with high, intermediate, and low variability, although significant differences can be seen upon examination of individual regions. Barnier et al. (2006) demonstrate the improved performance of the eddy-permitting global  $1/4^\circ$  ORCA025 model (used in Figure 1c) when partial-step topography and an energy-entropy conserving scheme for momentum are used (also used in the eddy-resolving  $1/12^\circ$  simulation).

In many regions, the variability in the  $1/4^\circ$  simulation is comparable to that in the  $1/12^\circ$  simulation and the altimeter map, even though it is eddy-permitting. However, the  $1/12^\circ$  simulation exhibits higher variability in ocean interiors and in some western boundary current systems, such as the Gulf Stream and North Atlantic Current, the Gulf of Mexico eddy-shedding, and the East Australian Current. In many ocean interior regions, the SSH variability in the  $1/12^\circ$  Mercator simulation exceeds that in

the altimetry map, which has  $1/3^\circ$  resolution and was calculated from altimeter data with track spacing generally  $> 1/12^\circ$ . In much of the Antarctic Circumpolar Current, the variability in the  $1/4^\circ$  simulation exceeds that in the altimetry map (and the  $1/12^\circ$  simulation), an issue discussed in Barnier et al. (2006). The success of the  $1/12^\circ$  Mercator in simulating the variability associated with the Agulhas retroflexion at the southern tip of Africa is particularly noteworthy (Figure 2f versus 2e) because that has

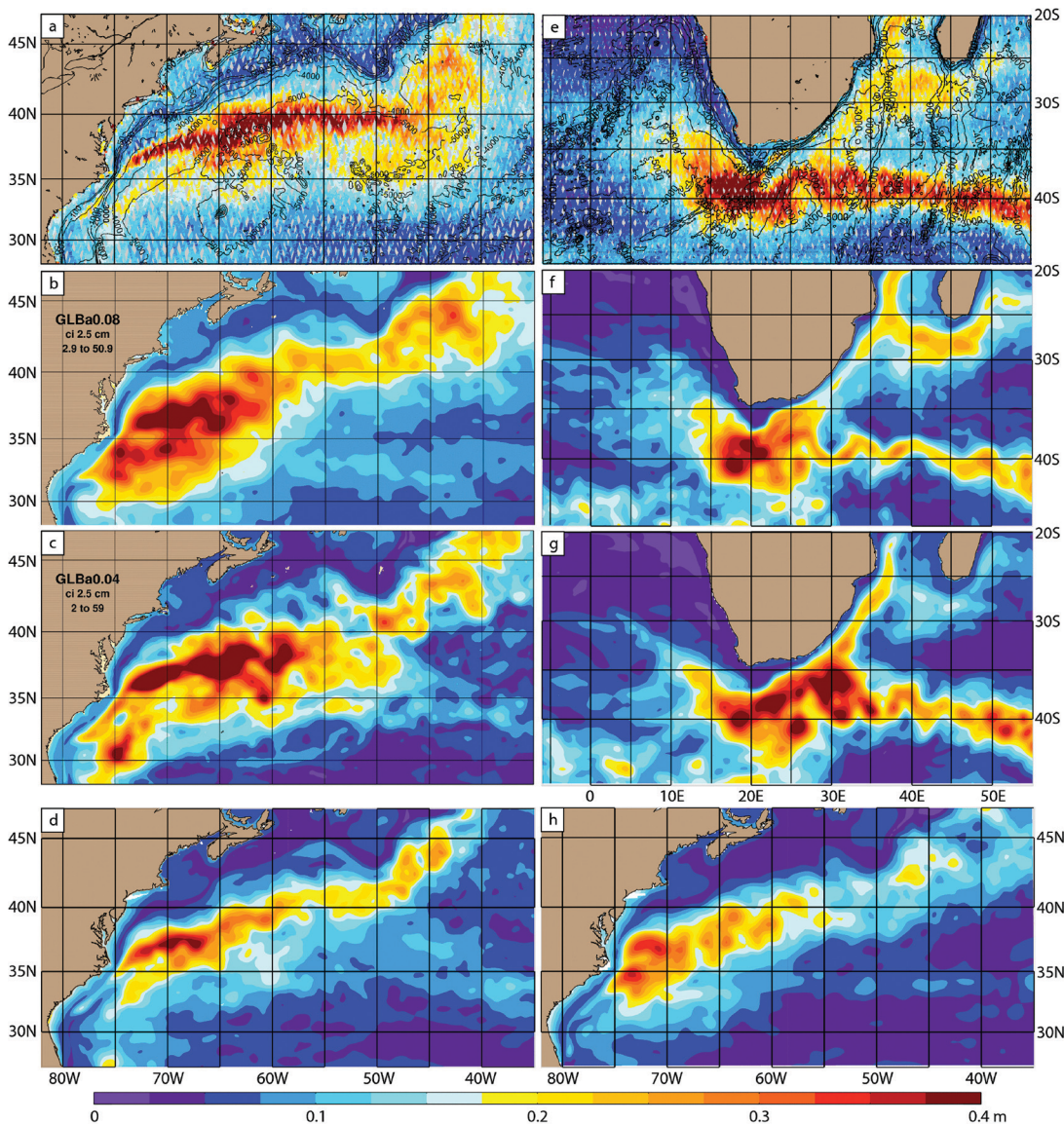


Figure 2. Zooms on (a–d, h) the Gulf Stream and (e–g) Agulhas retroflexion regions. (a,e) Along-track RMS SSH variability from satellite altimeter data in four orbits (available over the time window 2001–April 2008) overlaid on topographic contours (depth in meters) in (a) the Gulf Stream and (e) Agulhas retroflexion regions. The tracks are overlaid in the following order from top to bottom: (1) Envisat, (2) GFO, (3) Jason-1, and (4) TOPEX inter-leaved. (b,c) RMS SSH variability over (b) four model years and (c) model year 3 from nonassimilative (b)  $1/12^\circ$ , and (c)  $1/25^\circ$  global HYbrid Coordinate Ocean Model (HYCOM) simulations with 32 hybrid layers in the vertical and climatological atmospheric forcing from ECMWF with wind speed corrected using QuikSCAT climatology. Panels (d) and (f) are from the  $1/12^\circ$  and (g,h) from the  $1/4^\circ$  global Mercator simulations in Figure 1 for (d,h) the Gulf Stream region and (f,g) the Agulhas retroflexion region.



been a difficult feat for global ocean models. Unlike the observed variability, the models typically simulate preferred corridors for the eddies shed from the Agulhas retroflection, a tendency exhibited in the  $1/4^\circ$  Mercator simulation (Figure 2g versus 2e), but one that is often much stronger, even in eddy-resolving models (Barnier et al., 2006).

Even eddy-resolving ocean models exhibit significant discrepancies in simulating the ocean, for example, excessively high SSH variability in the northern half of the South China Sea ( $\sim 10\text{--}20^\circ\text{N}$ ,  $110\text{--}120^\circ\text{E}$ ) and maximum SSH variability in the Kuroshio region that is too far north immediately east of Japan in the  $1/12^\circ$  Mercator simulation (Figure 1b). Realistic simulation of the Gulf Stream is notoriously difficult, including its separation from the coast, its pathway to the east, and attaining sufficient eastward penetration as an inertial jet with associated high variability (Bryan et al., 2007; Chassignet and Marshall, 2008). Because there is particular interest in nowcasting and forecasting the mesoscale variability in this challenging region, Figure 2 includes a zoom focusing on the Gulf Stream. This zoom is a comparison among (a) along-track SSH variability from satellite altimeters in four orbits and SSH variability from four ocean model simulations without data assimilation, (b)  $1/12^\circ$  and (c)  $1/25^\circ$  global HYbrid Coordinate Ocean Model (HYCOM) simulations with climatological forcing, and the (h)  $1/4^\circ$  and (d)  $1/12^\circ$  Mercator simulations in Figure 1.

West of  $\sim 69^\circ\text{W}$ , the altimetry depicts a narrow band of high SSH variability along the Gulf Stream with very low variability north of the stream. The

reader is referred to Hurlburt and Hogan (2008) for an explanation of the Gulf Stream pathway and the related narrow band of high variability in this region, plus the dynamics required to obtain

is centered over the northwesternmost relatively flat topography in the region (not shown). The  $1/12^\circ$  Mercator and the  $1/25^\circ$  HYCOM simulate the most realistic patterns of variability in this

“THE NEED FOR ACCURATE PREDICTION OF OCEAN FEATURES THAT ARE INADEQUATELY OBSERVED, SUCH AS MIXED LAYER DEPTH, PLACES A MAJOR BURDEN ON THE OCEAN MODEL, DATA ASSIMILATION, AND ATMOSPHERIC FORCING.”

them. This explanation is strongly supported by observational evidence. The corresponding variability in the  $1/4^\circ$  Mercator simulation is characteristic of eddy-permitting ocean models, which tend to simulate an unrealistic mean northward meander just east of Gulf Stream separation from the coast, a phenomenon also seen in some eddy-resolving simulations (Barnier et al., 2006; Bryan et al., 2007; Hurlburt and Hogan, 2008) and discussed dynamically in the third reference. In the same region, the  $1/12^\circ$  HYCOM simulation exhibits a mean Gulf Stream pathway that is only slightly too far south and lies along the northern edge of a baroclinically unstable recirculation gyre with a narrow north-south extent ( $\sim 2^\circ$ ) (not shown). This gyre is inconsistent with observational evidence and gives rise to the unrealistically large area of high variability in this subregion, a general pattern of variability also seen in other eddy-resolving ocean models without the unrealistic northward meander after separation (Bryan et al., 2007). An eddy-driven mean abyssal gyre lies directly beneath the surface gyre and

subregion, but with high variability that still extends too far north. In addition,  $1/12^\circ$  Mercator and  $1/25^\circ$  HYCOM simulate a more realistic associated mean abyssal circulation (not shown) in comparison to observations (Pickart and Watts, 1990; Johns et al., 1995) and the dynamical explanation presented in Hurlburt and Hogan (2008), but simulate a key abyssal current near  $68.5^\circ\text{W}$  that is weaker than observed.

Although the  $1/12^\circ$  HYCOM does simulate the high variability associated with the Mann Eddy ( $\sim 48\text{--}40^\circ\text{W}$ ,  $40\text{--}46^\circ\text{N}$ ), otherwise the SSH variability in the  $1/12^\circ$  HYCOM and the  $1/4^\circ$  and  $1/12^\circ$  Mercator simulations is too low east of  $60^\circ\text{W}$  and even though both  $1/12^\circ$  HYCOM and  $1/12^\circ$  Mercator simulate an eastern nonlinear recirculation gyre, both completely miss the high SSH variability that wraps around it in Figure 2a ( $\sim 57\text{--}40^\circ\text{W}$ ,  $35\text{--}41^\circ\text{N}$ ), a feature discussed in Hurlburt and Hogan (2000). In the Year 3 (one-year) mean after initialization from climatology, the  $1/25^\circ$  global HYCOM simulation is spinning up toward a statistical equilibrium

for mesoscale variability, but the area of high variability is beginning to extend east of 60°W and the broader and more realistic north-south extent is evidence that a strong eastern recirculation gyre is forming.

### REAL-TIME VERIFICATION OF NOWCAST MESOSCALE VARIABILITY USING DROGUED DRIFTERS

Approximately 1250 drifters drogued at 15 m are deployed throughout the world ocean and report real-time data typically 16–20 times a day (Lumpkin and Pazos, 2007; National Oceanic and Atmospheric Administration, 2008). Their trajectories provide a powerful means of visual verification of specific features depicted in ocean prediction systems nearly anywhere in the world ocean. In Figure 3, four drifters in the East Australian Current (EAC) system are used to evaluate the depiction of mesoscale variability in the form of currents overlaid on SSH. The EAC is a western boundary current that is observed to be less coherent than other currents, such as the Kuroshio, Gulf Stream, and Agulhas, and is frequently observed to consist of many eddies (Ridgeway and Dunn, 2003). The results shown are from the Australian BLUElink> operational prediction system (Brassington et al., 2007) and ocean reanalysis system (Schiller et al., 2008), which are based on the Geophysical Fluid Dynamics Laboratory Modular Ocean Model version 4 (MOM4) (Griffies et al., 2004) and the BLUElink> ocean data assimilation system (BODAS; Oke et al., 2008), which uses ensemble optimal interpolation. The BLUElink> system is global, but eddy-resolving ( $1/10^\circ$ ) only in a  $90^\circ$  sector

surrounding Australia.

Figure 3a and 3b are for the same date (March 8, 2007). Figure 3a is from the reanalysis that uses a symmetric data window about the analysis date, while Figure 3b is a nowcast that only uses data prior to the analysis time. Both depict generally similar mesoscale features, but with significant differences. Two of the drifters move in tandem for six weeks, here circling near the center of an anticyclonic eddy seen in both analyses. A third drifter is moving southward past Coffs Harbour and Port Macquarie in the EAC, again in general agreement with both analyses. Figure 3b,c,d depicts a sequence of nowcast states one week apart (b) March 8, 2007, (c) March 15, 2007, and (d) March 22, 2007. In Figure 3c and 3d, the drifters traveling in tandem continue to circle an eddy that propagates offshore. The offshore propagation is not well captured in the nowcast. Instead, it depicts a nearshore eddy that propagates southward and an offshore eddy that strengthens, and highlights a specific instance where forecast skill can be significantly shortened when encountering complex eddy dynamics. The offshore propagation is better represented in the reanalysis (sequence not shown but represented for one date in Figure 3a), indicating that for complex flows, the real-time observation coverage can limit the quality of the nowcast, and thus forecast skill as well. The drifter in the EAC continues rapidly southward during the first week and shows that the nowcast captures the cyclone/anticyclone pair along the coast between  $34^\circ$  and  $38^\circ$ S. In Figure 3d, it returns toward the north followed by a fourth drifter that almost exactly overlays a trajectory segment of the third drifter.

The reversal of the arrow on the fourth drifter trajectory indicates a tight loop before it subsequently moves toward the southeast. Because the drifter data are Lagrangian, are available in real time, and the trajectory data are generally not assimilated by GODAE prediction systems, they represent an independent data set that can be routinely used for rapid assessment of mesoscale mapping by ocean prediction systems, especially the positioning of mesoscale eddies.

### A 10-DAY FORECAST DEMONSTRATION FOR THE GULF STREAM

Despite their shortcomings, the  $1/12^\circ$  global Mercator and HYCOM simulations both exhibit quite realistic mean Gulf Stream pathways (not shown) that are consistent with the present state of the art for eddy-resolving ocean general circulation models with high vertical resolution (Bryan et al., 2007; Chassignet and Marshall, 2008). In addition, significant progress has been made in nowcasting and forecasting the Gulf Stream as illustrated in Figure 4, where 10-day forecasts of current speed (at 15-m depth for April 26, 2008) obtained from three different Mercator Océan prediction systems are compared with ocean color from the Moderate Resolution Imaging Spectroradiometer (MODIS). All three use the Nucleus for European Modelling of the Ocean (NEMO) model (Madec, 2008) and the SAM2 data assimilation scheme based on the singular evolutive extended Kalman (SEEK) filter (Brasseur and Verron, 2006), but in the  $1/12^\circ$  Atlantic and the  $1/4^\circ$  global, the analysis correction is applied as a single increment at the time



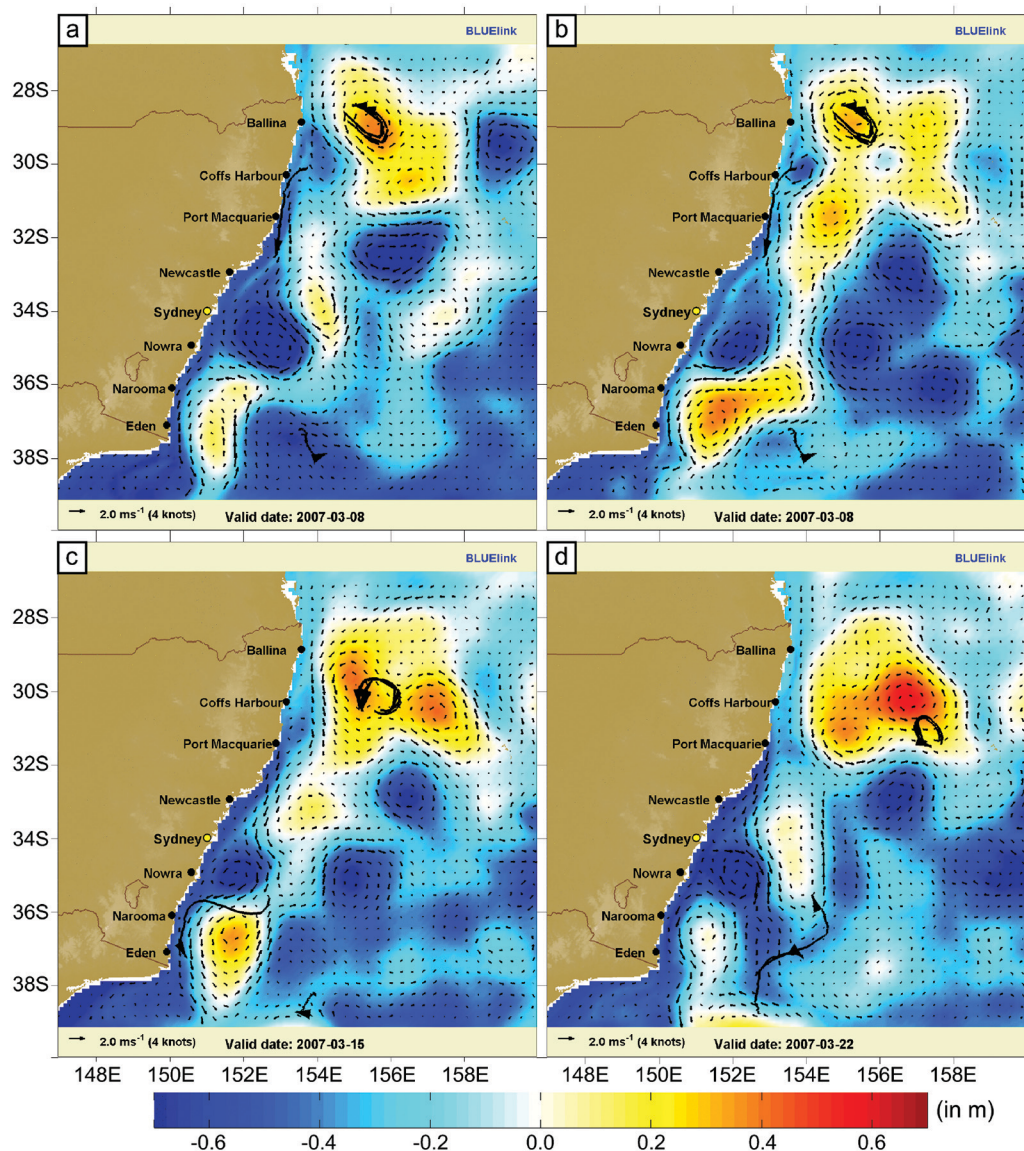


Figure 3. Snapshots of SSH in the East Australian Current region with ocean current vectors and observed  $\pm 2$ -day drifter trajectories overlaid. All are from the Australian BLUElink> global ocean prediction system. This system has  $1/10^\circ$  resolution in the region around Australia ( $90^\circ\text{E}$ – $180^\circ\text{E}$ ,  $75^\circ\text{S}$ – $16^\circ\text{N}$ ) and uses the Geophysical Fluid Dynamics Laboratory Modular Ocean Model version 4 (MOM4) with multivariate ensemble optimal interpolation data assimilation. (a) is from a reanalysis that uses data on both sides of the analysis date, while (b–d) are from the operational real-time system that only uses data up to the analysis date. (a) and (b) are for March 8, 2007, (c) for March 15, 2007, and (d) for March 22, 2007.

of analysis, while the  $1/12^\circ$  global uses an incremental analysis update (IAU) applied over the week following the analysis date. Two other articles in this issue provide additional information about GODAE-related ocean prediction systems (Dombrowsky et al.) and the data assimilation techniques employed (Cummings et al.), including Mercator and the other prediction systems discussed in this article.

It is readily apparent that the

$1/12^\circ$  eddy-resolving systems depict much more mesoscale variability and smaller scale features than the  $1/4^\circ$  eddy-permitting system (Figure 4b,c,d). In addition, currents tend to be stronger in the  $1/12^\circ$  systems. In the MODIS ocean color (Figure 4a), the heavy black line is designed to mark the ocean color front along the northern edge of the Gulf Stream and its initial turn to the north (up to  $44^\circ\text{N}$ ) as the North Atlantic Current. This front is overlaid on the

three model forecasts as are 10-day trajectories of drifters drogued at 15 m. A strong eddy is depicted near  $38^\circ\text{N}$ ,  $73^\circ\text{W}$ , close to the location where the Gulf Stream separates from the coast. This feature is captured only in the forecast by the  $1/12^\circ$  Atlantic system, which depicts it as a sharp current meander with approximately a  $1^\circ$  displacement error in comparison to the overlaid front. Three of the drifter trajectories lie close to the front, including one that

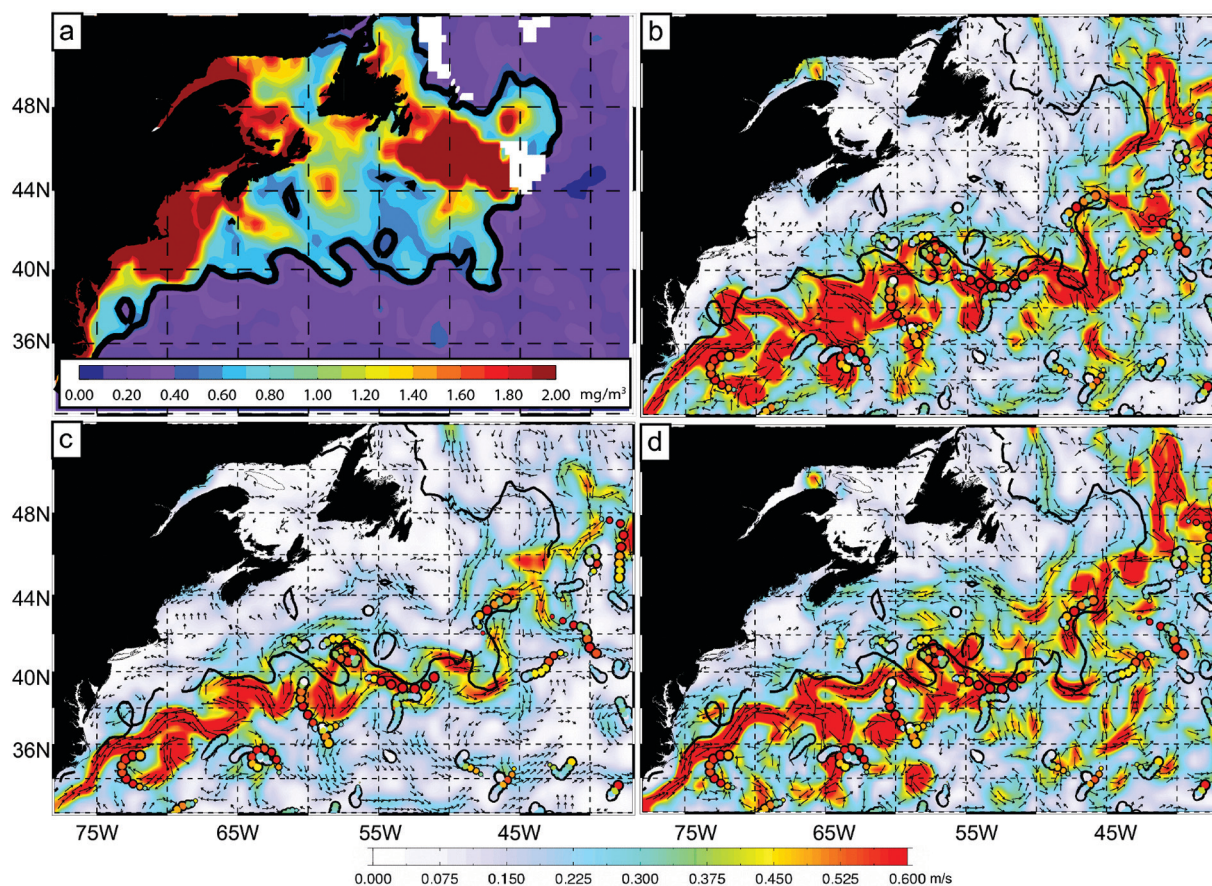


Figure 4. (a) Chlorophyll-*a* concentration latest cloud-free pixel composite from Moderate Resolution Imaging Spectroradiometer (MODIS) for the week ending April 26, 2008. The thick black line is the  $0.5 \text{ mg m}^{-3}$  contour, which tends to follow the Gulf Stream front. (b–d) 10-day ocean current forecasts at 15-m depth valid on April 26, 2008, from three Mercator Océan prediction systems, (b) the  $1/12^\circ$  Atlantic and Mediterranean system, (c) the  $1/4^\circ$  global system, and (d) the  $1/12^\circ$  global system, all overlaid with the black line from (a) and with 10-day (April 20–29, 2008) trajectories from drifters drogued at 15 m. Drifter speed along a trajectory is indicated by the color bar also used for the speed of the forecast ocean currents. The sizes of the circles representing the drifter trajectories decrease with data age.

indicates a closed circulation within a frontal meander. All three show good agreement with the front and depict the appropriate direction of flow along it, except for the oldest data (the end with the smallest circles). The three forecasts show the Gulf Stream generally flowing along the south side of the front with varying levels of agreement along the pathway, but with similar levels of agreement overall. All three systems also depict a current flowing anticyclonically along the northern and eastern edge of

the high chlorophyll feature centered near  $47^\circ\text{N}$ ,  $45^\circ\text{W}$  in general agreement with the overlaid front. In all three systems, current directions are in general agreement with the most recent half of the drifter trajectories about 60% of the time. Thus, despite differences, evidence of 10-day forecast skill for specific features in the Gulf Stream region can be found in the Mercator Océan prediction systems by comparing the forecasts with the ocean color image and drifter trajectories.

## EXPLORING THE TIME SCALE FOR OCEAN WEATHER PREDICTION SKILL

The real-time pre-operational  $1/12^\circ$  global HYCOM prediction system (Hurlburt et al., 2008a; Chassignet et al., 2009) includes the Navy Coupled Ocean Data Assimilation (NCODA) (Cummings, 2005) system with multivariate optimum interpolation (MVOI; Daley, 1991) for data assimilation and atmospheric forcing from the Navy Operational Global Atmospheric



Prediction System (NOGAPS; Rosmond et al., 2002). Ocean model dynamical interpolation skill plays an important role in the data assimilation process, a topic discussed and illustrated in Shriver et al. (2007) and Hurlburt et al. (2008a, 2009). In Figure 5, the 1/12° global HYCOM system is used to investigate the feasibility of forecast skill on time scales up to a month, well beyond the nominal one-week time scale for atmospheric predictive skill. Forecast skill over the global ocean (in the latitude range 45°S–45°N) and in several subregions is illustrated in Figure 5a–f. In each panel, three forecasts are verified using anomaly correlation between forecast SSH and the nowcast for the same date. The green line shows anomaly correlation when analysis-quality atmospheric forcing is used throughout the forecast, the red line indicates when the atmospheric forcing reverts toward climatology after five days (termed operational forcing), and the blue line represents a forecast of persistence. In five regions (Figure 5a–e), the forecast skill (anomaly correlation > .6) extends well beyond the time scale for atmospheric prediction skill and is only moderately degraded by the use of operational forcing. The Yellow/Bohai Sea is a notable exception. In that region, a forecast of persistence loses skill in less than two days. Skill is also rapidly lost when atmospheric forcing reverts toward climatology. However, the anomaly correlation remains very high as long as analysis quality forcing is used.

Hurlburt et al. (2008a) discuss ocean prediction skill in relation to classes of response to atmospheric forcing. The Yellow/Bohai Sea is very shallow. In shallow water and the surface mixed

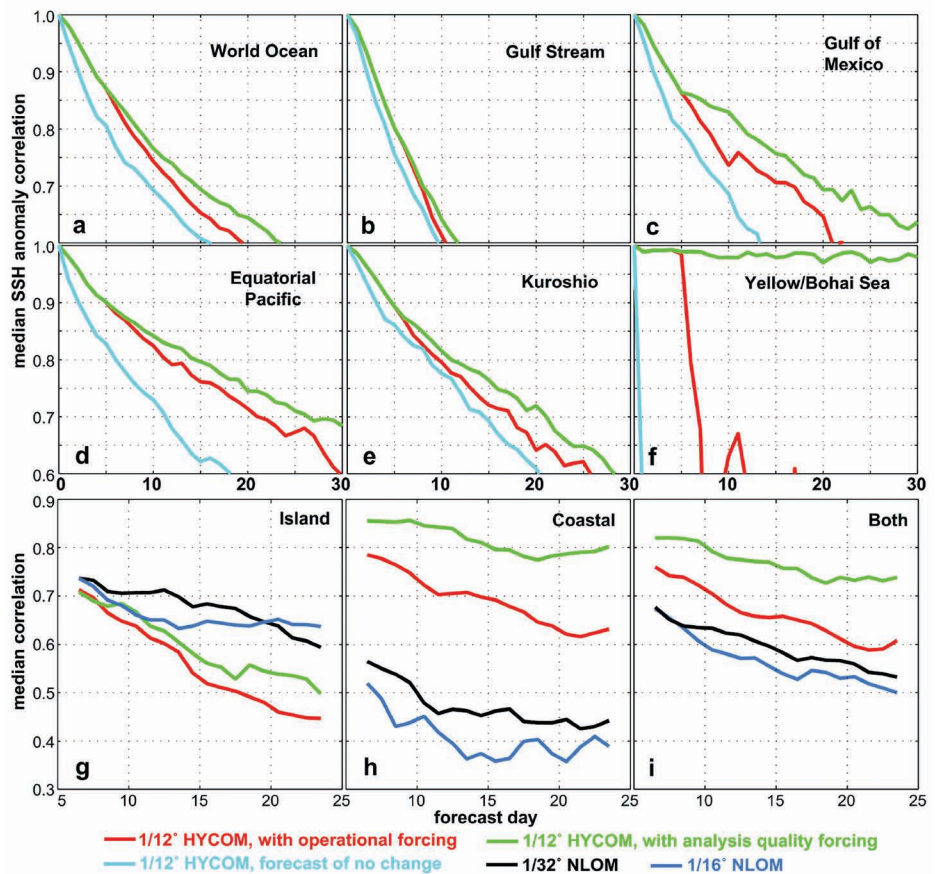


Figure 5. Verification of 30-day ocean forecasts. (a–f) Median SSH anomaly correlation of HYCOM forecasts versus forecast length in comparison with the verifying analysis for (a) the global domain (45°S–45°N) and five subregions (b–f) defined in Table 1. The red curves verify forecasts using operational atmospheric forcing that reverts toward climatology after five days. The green curves verify “forecasts” with analysis-quality forcing for the duration, and the blue curves verify forecasts of persistence (i.e., no change from the initial state). The plots give median statistics over twenty 30-day forecasts initialized during the period from January 2004 through December 2005, a period when data from three nadir-beam altimeters were assimilated. The same HYCOM forecasts and twenty-two 30-day Naval Research Laboratory Layered Ocean Model (NLOM) forecasts from June 2001–June 2002 were used to obtain (g–i) median correlation between forecast and observed SSH fluctuations from 1/12° HYCOM with operational forcing during the forecast (red lines), 1/12° HYCOM with analysis quality forcing for the duration (green lines), 1/16° (blue lines), and 1/32° (black lines) NLOM (both with operational atmospheric forcing) at (g) 23 (49) open ocean island tide gauge stations for HYCOM (NLOM), (h) 91 (29) coastal tide gauges for HYCOM (NLOM), and (i) all 114 (78) tide gauges for HYCOM (NLOM). A 13-day moving average was applied to filter time scales not resolved by the altimeter data. Tide gauge SSH data are not assimilated by the ocean prediction systems. Some results are adapted from Hurlburt et al. (2008a) and Shriver et al. (2007). Also see Chassignet et al. (2009).

Table 1. Regional boundaries of the subregions depicted in Figure 5

Subregion name	Latitude range	Longitude range
Gulf Stream region	35°N–45°N	76°W–40°W
Gulf of Mexico	18.2°N–32.6°N	98°W–79°W
Equatorial Pacific	20°S–20°N	109.1°E–77.2°W
Kuroshio	20.1°N–54.9°N	120.2°E–179.4°W
Yellow/Bohai Sea	30°N–42°N	118°E–127°E

layer (e.g., SST and mixed layer depth), the ocean responds rapidly to atmospheric forcing and the forecast rapidly becomes more sensitive to atmospheric forcing than the initial state. In contrast,

Ocean Model (NLOM) simulations (without ocean data assimilation) have more realistic dynamics and increased simulation skill in the Gulf Stream region than comparable  $1/16^\circ$  NLOM

the models and prediction systems.

There are significant pitfalls in using model nowcasts to verify model forecasts. For example, decreases in input data could lead to apparent increases in forecast skill because the evolution of the nowcast was less constrained by data.

In addition, coarser-resolution models could demonstrate greater forecast skill than finer-resolution models because of smoother, larger-scale features that became out of phase more slowly.

However, in these models, persistence would also generally indicate greater skill, and the spread between the forecast and persistence for a given forecast length would be smaller. Therefore, when prediction system resolution is increased, an increased difference between the anomaly correlation of the forecast and the (lower) anomaly correlation of persistence is a better indicator of increased forecast skill than the anomaly correlation of the forecast alone (Shriver et al., 2007). In the Gulf Stream region, the  $1/32^\circ$  global NLOM system gives a 37% increase in forecast skill over the corresponding  $1/16^\circ$  system based on the increased temporal spread between the model forecast skill and that of persistence (at an anomaly correlation of 0.6).

In addition, the preceding pitfalls highlight the need to use independent, unassimilated data sets in assessing forecast skill. In Figure 5g,h,i, unassimilated tide gauge data are used to assess model skill in forecasting SSH. For this purpose, forecast skill is assessed against island and coastal tide gauge stations separately, as well as combined. HYCOM forecasts with both analysis-quality forcing (green lines) and operational forcing (red lines) are assessed. NLOM  $1/16^\circ$  (blue lines) and  $1/32^\circ$  (black lines)

“...THE TIME SCALE FOR “OCEAN WEATHER” PREDICTIVE SKILL IS INFLUENCED BY A NUMBER OF FACTORS, SUCH AS OCEAN DYNAMICS, THE ABILITY OF THE OCEAN MODEL TO SIMULATE THE ESSENTIAL DYNAMICS, AND ATMOSPHERIC FORCING.”

mesoscale variability in the deep ocean is largely nondeterministic in relation to atmospheric forcing due to flow instabilities. Thus, the time scale for predictive skill depends more on the quality of the initial state, the accuracy of the model dynamics, and the time scale of the flow instabilities than on the atmospheric forcing. Forecast skill in the Gulf of Mexico is second most affected by using operational forcing because of its broad, shallow shelf regions.

The Gulf Stream is particularly difficult to forecast and the 10-day Gulf Stream forecasts from Mercator (Figure 4) are right at the limit of useful forecast skill in HYCOM (Figure 5b). Earlier, we identified some shortcomings in  $1/12^\circ$  global HYCOM and Mercator dynamics and simulation skill in the Gulf Stream region (without ocean data assimilation). Would improved simulation skill yield improved forecast skill in the region? Based on extensive model-data comparisons, Hurlburt and Hogan (2000, 2008) demonstrate that  $1/32^\circ$  (3.5-km resolution) NRL Layered

simulations. Correspondingly, the  $1/32^\circ$  global NLOM prediction system yields median 15-day forecast skill in the Gulf Stream region (Hurlburt et al., 2008a). The  $1/16^\circ$  and  $1/32^\circ$  global NLOM systems have high horizontal resolution, but only seven Lagrangian layers in the vertical, including the mixed layer. Shriver et al. (2007) describe the NLOM systems, their assimilation of SSH and SST, and their use of NOGAPS atmospheric forcing. The SSH assimilation consists of an optimum interpolation (OI) deviation analysis from the model first guess and an empirical orthogonal function regression technique based on model statistics to project SSH updates downward, including to the abyssal layer (Hurlburt et al., 1990) with geostrophic balancing outside an equatorial band and IAU over a one-day interval. Because HYCOM and Mercator are inherently more accurate in ocean model design, there is opportunity for even greater forecast skill in the Gulf Stream and other regions, as model resolution is increased and improvements are made to



forecasts with operational forcing are also assessed. A 13-day moving average was applied to the SSH time series to filter time scales not resolved by the altimeter data. Analysis-quality forcing has much greater impact on forecast skill at the coastal stations than the island stations, as expected based on the earlier discussion. At the coastal stations, the NLOM forecasts are clearly inferior to the HYCOM forecasts because NLOM does not include shallow water or shallow-water dynamics, and the nearest HYCOM grid point is generally closer to the coastal tide gauge than the nearest NLOM grid point. At the island stations, the NLOM forecasts appear to have an edge over HYCOM, but different time periods and some different tide gauges were used in assessing HYCOM and NLOM forecast skill, so only large differences are meaningful. In both cases, the  $1/32^\circ$  NLOM forecasts generally outperform the  $1/16^\circ$  NLOM forecasts, confirming the value of increased resolution based on independent data.

### LONGER-RANGE FORECASTS OF KUROSHIO MEANDERS SOUTH OF JAPAN

In Figure 5,  $1/12^\circ$  global HYCOM demonstrates longer-range forecast skill for the Kuroshio region than for the Gulf Stream region. As discussed earlier, the time scale for “ocean weather” predictive skill is influenced by a number of factors, such as ocean dynamics, the ability of the ocean model to simulate the essential dynamics, and atmospheric forcing. In this example, ocean model dynamics and the ability to simulate them are significant factors. In the Gulf Stream region, both  $1/12^\circ$  HYCOM and  $1/12^\circ$  Mercator (without ocean data

assimilation) demonstrated deficiencies in model dynamics and simulation skill, as evidenced earlier in the section on “Need For An Eddy-Resolving Ocean Model.” In contrast, simulations without ocean data assimilation performed using the Japanese  $1/10^\circ$  Meteorological Research Institute Community Ocean Model (MRI.COM) and  $1/12^\circ$  HYCOM have demonstrated greater skill in representing key features of the Kuroshio and their dynamics (Tsujino et al., 2006; Hurlburt et al., 2008b).

Based on relatively long time scales for the evolution of Kuroshio meanders south of Japan observed by Ambe et al. (2004) (longer than typical of the much larger Kuroshio region used for HYCOM forecast verification in Figure 5e) plus the  $1/10^\circ$  MRI.COM simulation skill and realistic dynamics for such features demonstrated by Tsujino et al. (2006), Usui et al. (2006) used this model to investigate the potential for longer-range forecasts of these features. In particular, they performed a hindcast and 138 90-day forecasts initialized from the hindcast on the first day of each month from February 1, 1993 to July 1, 2004. The model domain covers a large part of the northwestern Pacific ( $15^\circ\text{N}$ – $65^\circ\text{N}$ ,  $117^\circ\text{E}$ – $160^\circ\text{W}$ ) with resolution of  $1/6^\circ$  to  $1/10^\circ$ , and  $1/10^\circ$  resolution covering  $15^\circ\text{N}$ – $50^\circ\text{N}$ ,  $117^\circ\text{E}$ – $160^\circ\text{E}$ . This model is nested in an MRI.COM Pacific model spanning  $15^\circ\text{S}$ – $65^\circ\text{N}$  with  $1/2^\circ$  resolution. Both have 54 levels in the vertical and use a multivariate three-dimensional variational (3DVAR) analysis scheme to assimilate along-track satellite altimeter data and temperature and salinity profiles. The reader is referred to Dombrowsky et al. (2009) for more information about the prediction

systems, Tsujino et al. (2006) for more information about the model, and Usui et al. (2006) for more information about the analysis and data assimilation.

For the purpose of the 90-day forecast, a relatively long data window (one-third of a month) is used for each 3DVAR analysis and the IAU technique of Bloom et al. (1996) is used to update model fields over the same period as the data window, an approach that tends to suppress short time scales compared to  $1/12^\circ$  global HYCOM that uses a one- to three-day data window and a six-hour IAU window to update the model. In addition, analysis-quality atmospheric forcing from the National Centers for Environmental Prediction (NCEP2) reanalysis (Kanamitsu et al., 2002) was used for the hindcasts and for the duration of the 90-day forecasts.

Figure 6 depicts (a) the initial state plus (e) 25-day and (f) 55-day forecasts of the development of the largest Kuroshio meander that occurred south of Japan during the 1993–2004 time period of the study. The success of this forecast is verified by the corresponding data-assimilative hindcast state in Figure 6b and 6c. Typically, the skill of the 138 forecasts lasts 40–60 days, as demonstrated by comparing the average RMS error of the forecast SSH to error obtained from forecasts of persistence or climatology (Figure 6d). In each case, the hindcast was used as the truth. Some degradation of forecast skill would be expected if operational rather than analysis-quality atmospheric forcing was used during the 90-day forecasts, as seen in Figure 5, a decrease yet to be assessed.

As independent validation, hindcast near-surface velocity fields were compared to unassimilated acoustic

Doppler current profiler (ADCP) measurements along 137°E south of Japan. The correct location of the Kuroshio and much of the mesoscale eddy field is depicted in the example shown in Figure 7. The correlation between the zonal (meridional) velocity components is 0.84 (0.47). The preceding indications that the assimilation system is able to realistically represent both velocity and SSH are prerequisite for it to represent Kuroshio-eddy interaction and baroclinic instability processes associated with the development of the Kuroshio large meander, dynamics investigated by Tsujino et al. (2006) using the same model without data assimilation and by Usui et al. (2008a,b) using the data-assimilative 1993–2004 hindcast experiment.

## SST FORECASTING USING EDDY-RESOLVING OCEAN MODELS

In the future, it is likely that global ocean prediction systems will become components of Earth system prediction models (coupled atmosphere, ocean, ice, surface wave, land, and hydrological models) to greatly expand the predictive capability for the earth's environment and increase the time scale for useful predictive skill. Therefore, accurate SST nowcasting and forecasting is a particularly crucial capability for global ocean prediction models. Eddy-resolving global ocean prediction systems are advantageous for this application because of their ability to accurately map sharp ocean fronts and resolve the response to hurricanes and regions of coastal upwelling. Ocean

model SST can also respond to transient atmospheric forcing and provide estimates (a) in areas of precipitation and cloud cover, (b) under high and low wind conditions, (c) of diurnal variations, and (d) of surface layer entrainment and mixing.

Figure 8 presents an assessment of  $1/12^\circ$  daily weeklong SST forecasts by Mercator with forcing from the European Centre for Medium-Range Weather Forecasts atmospheric forecasts. Using comparisons to the corresponding nowcast as the metric, the one-day forecast error is small over most of the domain but relatively large along the Gulf Stream, a region with large SST gradients and high variability. After one week, relatively large error tends to be found along coastlines and in the region of

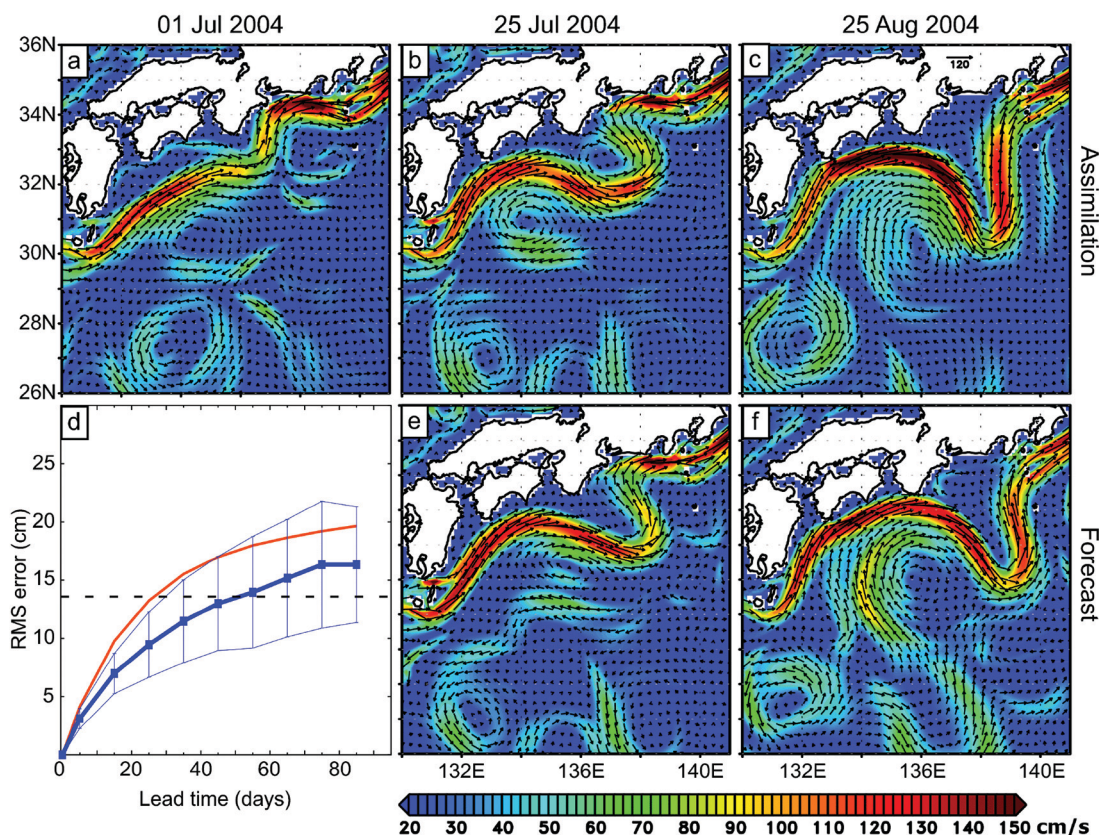


Figure 6. Prediction of the 2004 Kuroshio Large Meander in the Japan Meteorological Agency-Meteorological Research Institute (JMA-MRI) assimilative model. Panels (a–c) and (e–f) show the near-surface speed and velocity vectors. (a) Initial condition on July 1, 2004, (b) analysis on July 25, 2004, (c) analysis on August 25, 2004, (e) 25-day forecast valid July 25, 2004, and (f) 55-day forecast valid August 25, 2004. Units of the color bar are  $\text{cm s}^{-1}$  and the reference vector in panel (c) is  $120 \text{ cm s}^{-1}$ . Panel (d) is a predictability diagram showing RMS SSH error as a function of forecast length based on 138 forecasts over the time frame 1993–2004. RMS SSH error is calculated over the region  $131^\circ\text{--}140^\circ\text{E}$ ,  $30^\circ\text{--}35^\circ\text{N}$  south of Japan. Blue line: model forecast. Red line: persistence. Broken line: mean SSH variability, the error from using climatology as a forecast.

equatorial Atlantic upwelling. Upwelling is also prevalent in the area of large error just to the north along the coast of Africa (as well as other locations). The area of large SST error in the open Atlantic around 60°W, 30°N is the consequence of a hurricane and error in the forecast hurricane track. Figure 8c shows that, overall, the error in the SST forecasts is quite small and the forecasts are clearly superior to a forecast of persistence, the present approach used for SST in atmospheric forecast models. At present, the SST analyses used in atmospheric prediction systems are independent of an ocean model (see Donlon et al., 2009, about such analyses) and it is essential that SST nowcasts and forecasts by an ocean model demonstrate superiority over this approach. Success in predicting

SST depends heavily on the accuracy of the forecast atmospheric forcing and the ability of the parameterized physics used in the surface boundary layer of the ocean model to accurately represent key features, such as mixed layer depth, vertical temperature and salinity structure below the base of the mixed layer, and SST (Csanady, 2001; Kara and Hurlburt, 2006). In addition, it is necessary to include the effects of skin versus bulk SST under low wind conditions.

### COASTAL REGION PREDICTION USING LARGE-SCALE EDDY-RESOLVING OCEAN PREDICTION SYSTEMS

Another important attribute of eddy-resolving global and basin-scale ocean models is their ability to provide useful

resolution in coastal regions. These regions are of greatest interest to a majority of prediction system users. In addition, the eddy-resolving, large-scale models play an essential role in providing initial background and boundary conditions to even higher-resolution regional and coastal models that may include such capabilities as tides (with the tidal boundary conditions from a separate source) or an ecosystem component. Here, we use results from the Australian global BLUElink> system, described earlier, to illustrate the ability of an eddy-resolving prediction system to nowcast and forecast coastally trapped waves along the coast of Australia.

Figure 9a,b illustrates the impact of two coastally trapped waves on SSH and coastal currents as they propagate

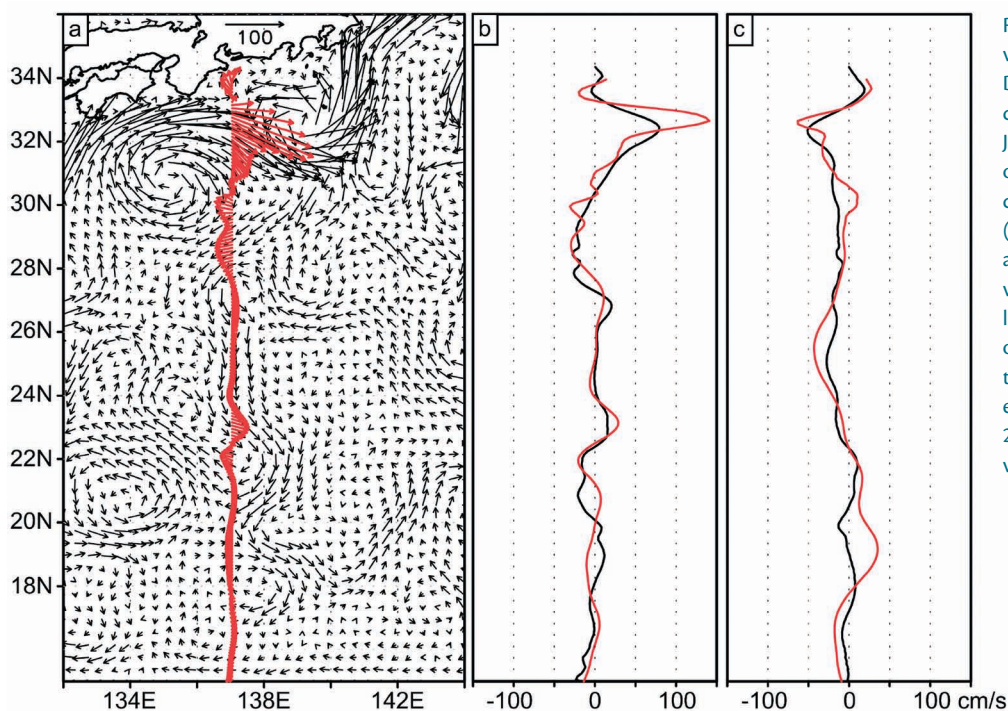


Figure 7. A comparison of near-surface velocity fields between independent acoustic Doppler current profiler observations collected during May 18–30, 2001, and the JMA-MRI assimilation experiment averaged over the same time interval. Panel (a) shows current vectors south of Japan, while panels (b) and (c) are zonal and meridional velocity along 137°E, respectively. The red (black) vectors and lines are the observations (assimilation experiment). The correlation coefficient of the zonal (meridional) velocity between the two data sets is 0.84 (0.47), based on eight repetitions of the line over the period 2001–2004. Units are  $\text{cm s}^{-1}$ , and the reference vector in panel (a) is  $100 \text{ cm s}^{-1}$ .



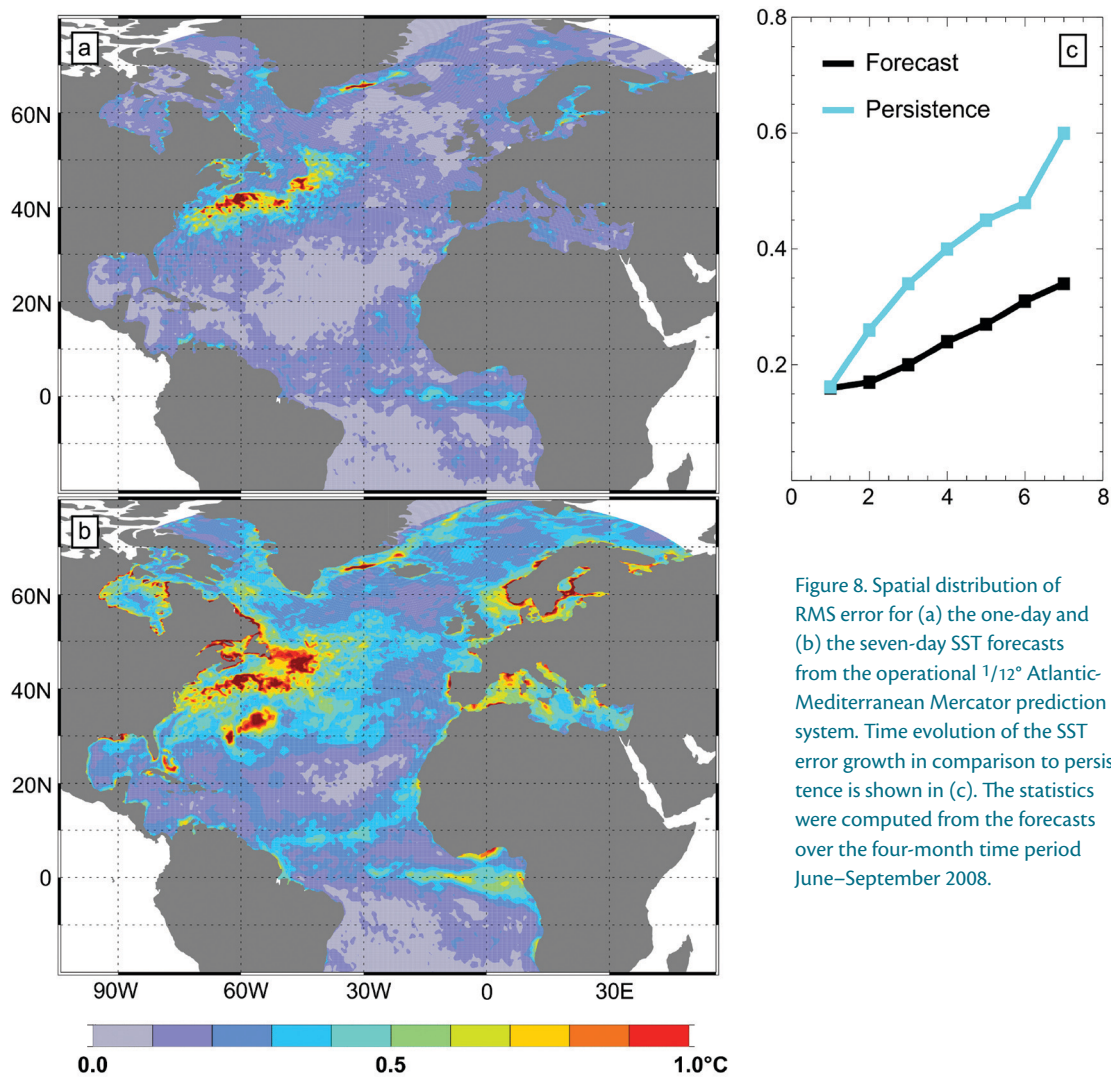


Figure 8. Spatial distribution of RMS error for (a) the one-day and (b) the seven-day SST forecasts from the operational  $1/12^\circ$  Atlantic-Mediterranean Mercator prediction system. Time evolution of the SST error growth in comparison to persistence is shown in (c). The statistics were computed from the forecasts over the four-month time period June–September 2008.

eastward along the south coast of Australia. These features are largely initiated by wind stress aligned such that a significant component of the mass transport accumulates at the coast. In the examples shown, storm surge is initiated by atmospheric cold fronts that propagate eastward from the Southern Ocean through the Great Australian Bight. Figure 9b is particularly interesting because it illustrates the bifurcation of a coastally trapped wave as it reaches the Bass Strait, which separates the Australian mainland and the island

of Tasmania. The Bass Strait is shallow and the portion of the wave propagating in shallow water passes through the strait, while the portion lying over deep water, farther offshore, passes south of Tasmania. At the same time the deep water coastally trapped wave reached the Derwent River (in southeast Tasmania), sea level was further amplified by a local storm. The superposition of the coastally trapped wave and the local storm surge is not represented in traditional storm surge models.

Remote coastally trapped waves

impact the currents, temperature, and salinity as well as sea level and are baroclinic phenomena not included in barotropic tide and storm-surge models. The Australian Bureau of Meteorology is using the BLUElink system to maintain a monitoring and forecast capability for these features that is verified by 10 tide gauge stations around Australia (Figure 9c). Figure 9d shows nowcast (day 0) and forecast verification statistics for up to six days at these 10 stations. This example illustrates the value of eddy-resolving global and basin-scale ocean



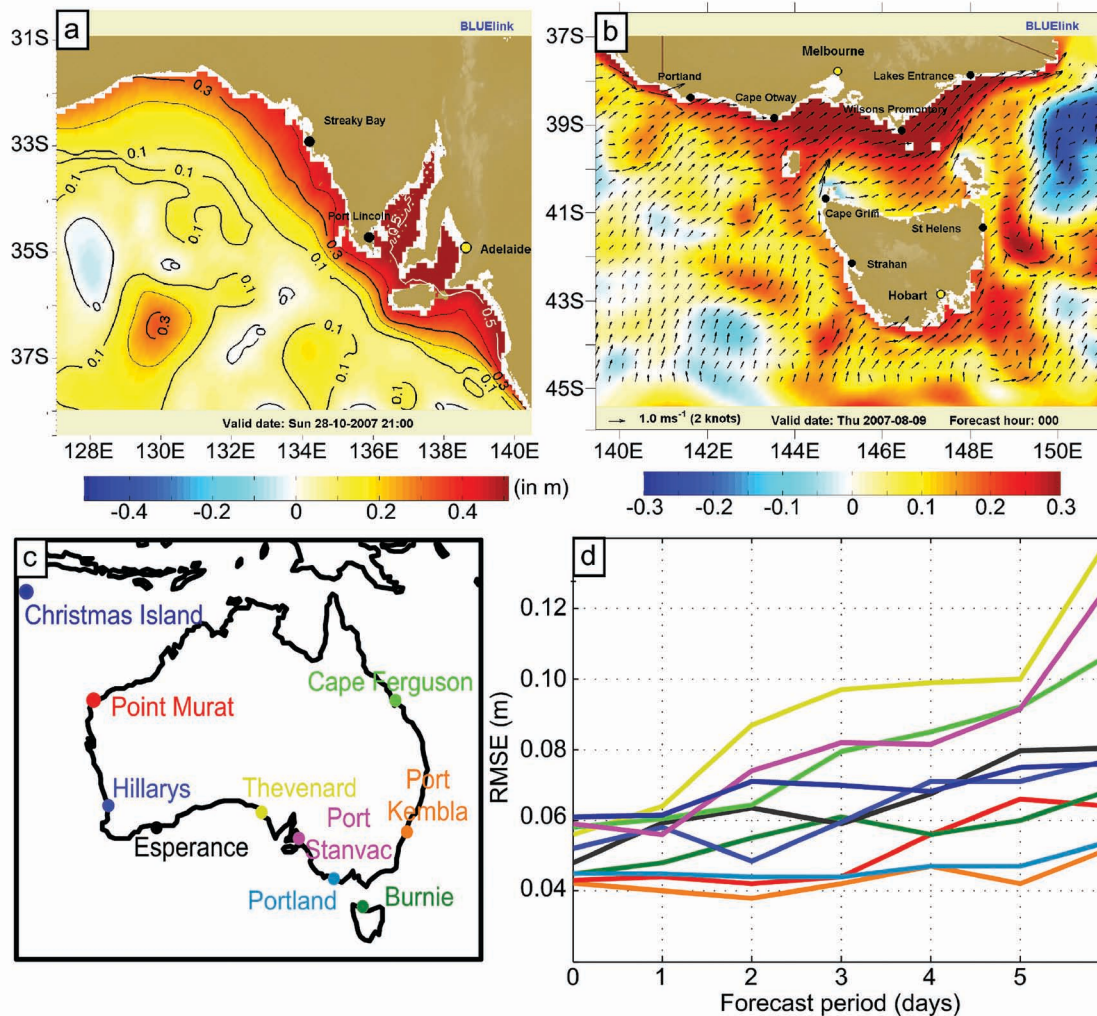


Figure 9. (a,b) Operational BLUElink> snapshots of two different coastally trapped waves propagating eastward along the south coast of Australia on (a) October 28, 2007, and (b) August 9, 2007. Panel (a) depicts SSH and (b) depicts SSH with current vectors overlaid. Panel (c) marks the locations of 10 tide gauge stations used in verifying (d) nowcasts (day 0) through six-day forecasts of coastally trapped waves.

prediction systems in providing crucial input for nested coastal models with even finer resolution, in this case coastally trapped waves that may originate outside the coastal model domain and propagate in through boundary conditions from the larger-scale model. Some of the longest and strongest coastally trapped waves are initiated in the equatorial wave guides of all three equatorial oceans and become coastally trapped waves upon reaching the eastern boundary, with those stemming from El Niño in the Pacific Ocean the best known example.

Other baroclinic phenomena that can also affect coastal sea level, currents, and temperature and salinity include boundary currents, eddies, upwelling/downwelling westward-propagating Rossby waves, hurricanes, and flows through straits. The ocean prediction system has the advantage that it can provide a total nontidal sea level with currents and temperature and salinity available from every forecast rather than as an event-based service, which may miss large anomalies composed of multiple, superposed processes. The

inclusion of external and internal tides in ocean prediction systems is a leading-edge topic and a significant challenge for ocean data assimilation of SSH. In the interim, a total sea level product can be obtained by combining highly accurate and tuned tidal harmonics with model predicted nontidal sea level.

## SUMMARY AND CONCLUSIONS

The feasibility of global and basin-scale high-resolution analyses and forecasts at the mesoscale has been illustrated by demonstrating several key capabilities.

The first was a demonstration of eddy-resolving global ocean modeling without ocean data assimilation, because an eddy-resolving model that performs well is a key component of a global prediction system for mesoscale ocean features, a point verified in subsequent examples. Nowcasting and forecasting of mesoscale variability by assimilation of satellite altimeter data is a key capability demonstrated in multiple examples, including the capability to verify specific mesoscale features using independent data and an

in future eddy-resolving global ocean prediction systems.


Although many of the results presented here are from reanalyses or hindcasts using historical data and archived atmospheric products, most of the ocean prediction systems themselves run routinely in an operational or pre-operational mode in real time or near-real time. The exceptions are  $1/12^\circ$  global Mercator and  $1/25^\circ$  global HYCOM, which provide demonstrations of future capabilities.

## “THE FEASIBILITY OF GLOBAL AND BASIN-SCALE HIGH-RESOLUTION ANALYSES AND FORECASTS AT THE MESOSCALE HAS BEEN ILLUSTRATED BY DEMONSTRATING SEVERAL KEY CAPABILITIES.”

exploration of the time scale for oceanic predictive skill in different dynamical regimes. Forecast skill on time scales up to about one month was demonstrated for mesoscale variability. A mesoscale example where even longer-range skill is possible was also demonstrated. Using forecast atmospheric forcing, forecast skill of at least one week was demonstrated for SST. That capability is essential for future coupled ocean-atmosphere prediction. Finally, nowcast/forecast skill was demonstrated in coastal regions for coastally trapped waves. That capability is especially important for user applications and for nested coastal models with even higher resolution. At present, tidal boundary conditions must be provided separately, but work has begun to include external and internal tides as an option

### ACKNOWLEDGEMENTS

The US effort was supported by the US GODAE: Global Ocean Prediction with the HYbrid Coordinate Ocean Model (HYCOM) project, funded under the National Ocean Partnership Program (NOPP); by the 6.1 project Global Remote Littoral Forcing via Deep Water Pathways, funded by the Office of Naval Research (ONR) under program element 601153N; and by grants of computer time from the US Defense Department High Performance Computing Modernization Program. The Australian BLUElink> science and technical team was supported by the Bureau of Meteorology, CSIRO, Wealth from Oceans National Research Flagship, and the Royal Australian Navy. The European high-resolution global

ocean system was developed in France by Mercator Océan with the financial support of the European MERSEA integrated project for the development, validation, and exploitation of the system and from the Région Midi Pyrénées, which financed a dedicated computer for this project. The Japanese GODAE effort was supported by JMA/MRI and by Category 7 of the MEXT RR2002 Project for Sustainable Coexistence of Humanity, Nature and the Earth. The Australian, French, Japanese, and US groups have all been active participants in GODAE, and GODAE has contributed greatly to the success of their global and basin-scale ocean prediction system development efforts. 

### REFERENCES

- Ambe, D., S. Imawaki, H. Uchida, and K. Ichikawa. 2004. Estimating the Kuroshio axis south of Japan using a combination of satellite altimetry and drifting buoys. *Journal of Oceanography* 60:375–382.
- Barnier, B., G. Madec, T. Penduff, J.-M. Molines, A.-M. Treguier, J. Le Sommer, A. Beckman, A. Biastoch, C. Böning, J. Dengg, and others. 2006. Impact of partial steps and momentum advection schemes in a global ocean circulation model at eddy-permitting resolution. *Ocean Dynamics* 56:543–567, doi:10.1007/s10236-006-0082-1.
- Bloom, S.C., L.L. Takacs, A.M. da Silva, and D. Ledvina. 1996. Data assimilation using incremental analysis updates. *Monthly Weather Review* 124:1,256–1,271.
- Brasseur, P., and J. Verron. 2006. The SEEK filter method for data assimilation in oceanography: A synthesis. *Ocean Dynamics* 56:650–661.
- Brassington, G.B., T. Pugh, C. Spillman, E. Schulz, H. Beggs, A. Schiller, and P.R. Oke. 2007. BLUElink> Development of operational oceanography and servicing in Australia. *Journal of Research and Practice in Information Technology* 39(2):151–164.
- Bryan, F.O., M.W. Hecht, and R.D. Smith. 2007. Resolution convergence and sensitivity studies with North Atlantic circulation models. Part I. The western boundary current system. *Ocean Modelling* 16:141–159.

- Chassignet, E.P., H.E. Hurlburt, E.J. Metzger, O.M. Smedstad, J. Cummings, G.R. Halliwell, R. Bleck, R. Baraille, A.J. Wallcraft, C. Lozano, and others. 2009. US GODAE: Global ocean prediction with the HYbrid Coordinate Ocean Model (HYCOM). *Oceanography* 22(2):64–75.
- Chassignet, E.P., and D.P. Marshall. 2008. Gulf Stream separation in numerical ocean models. Pp. 39–61 in *Ocean Modeling in an Eddy Regime*, Geophysical Monograph 177. M.W. Hecht and H. Hasumi, eds, American Geophysical Union, Washington, DC.
- Chelton, D.B., R.A. deSzoeke, and M.G. Schlax. 1998. Geographical variability of the first baroclinic Rossby radius of deformation. *Journal of Physical Oceanography* 28(3):433–460.
- Clark, C., and the In Situ Observing System Authors, and S. Wilson and the Satellite Observing System Authors. 2009. An overview of global observing systems relevant to GODAE. *Oceanography* 22(3):22–33.
- Csanady, G.T. 2001. *Air-Sea Interactions: Laws and Mechanisms*. Cambridge University Press, New York, 248 pp.
- Cummings, J.A. 2005. Operational multivariate ocean data assimilation. *Quarterly Journal of the Royal Meteorological Society* 131(613):3,583–3,604.
- Cummings, J., L. Bertino, P. Brasseur, I. Fukumori, M. Kamachi, M.J. Martin, K. Mogensen, P. Oke, C.E. Testut, J. Verron, and A. Weaver. 2009. Ocean data assimilation systems for GODAE. *Oceanography* 22(3):96–109.
- Daley, R. 1991. *Atmospheric Data Analysis*. Cambridge University Press, Cambridge, 457 pp.
- Dombrowsky, E., L. Bertino, G.B. Brassington, E.P. Chassignet, F. Davidson, H.E. Hurlburt, M. Kamachi, T. Lee, M.J. Martin, S. Mei, and M. Tonani. 2009. GODAE systems in operation. *Oceanography* 22(3):80–95.
- Donlon, C.J., K.S. Casey, I.S. Robinson, C.L. Gentemann, R.W. Reynolds, I. Barton, O. Arino, J. Stark, N. Rayner, P. LeBorgne, and others. 2009. The GODAE High-Resolution Sea Surface Temperature Pilot Project. *Oceanography* 22(3):34–45.
- Ducet, N., P.Y. Le Traon, and G. Reverdin. 2000. Global high-resolution mapping of ocean circulation from TOPEX/Poseidon and ERS-1 and -2. *Journal of Geophysical Research* 105(C8):19,477–19,498.
- Emery, W.J., W.G. Lee, and L. Magaard. 1984. Geographic and seasonal distributions of Brunt-Väisälä frequency and Rossby radii in the North Pacific and North Atlantic. *Journal of Physical Oceanography* 14:294–317.
- Griffies, S.M., M.J. Harrison, R.C. Pacanowski, and A. Rosati. 2004. *A Technical Guide to MOM4*. GFDL Ocean Group Technical Report No. 5, National Oceanic and Atmospheric Administration/Geophysical Fluid Dynamics Laboratory, Princeton, NJ, 339 pp.
- Hurlburt, H.E., and P.J. Hogan. 2000. Impact of  $1/8^\circ$  to  $1/64^\circ$  resolution on Gulf Stream model-data comparisons in basin-scale subtropical Atlantic Ocean models. *Dynamics of Atmospheres and Oceans* 32:283–329.
- Hurlburt, H.E., and P.J. Hogan. 2008. The Gulf Stream pathway and the impacts of the eddy-driven abyssal circulation and the Deep Western Boundary Current. *Dynamics of Atmospheres and Oceans* 45:71–101.
- Hurlburt, H.E., E.P. Chassignet, J.A. Cummings, A.B. Kara, E.J. Metzger, J.F. Shriver, O.M. Smedstad, A.J. Wallcraft, and C.N. Barron. 2008a. Eddy-resolving global ocean prediction. Pp. 353–381 in *Ocean Modeling in an Eddy Regime*, Geophysical Monograph 177. M.W. Hecht and H. Hasumi, eds, American Geophysical Union, Washington, DC.
- Hurlburt, H.E., Y. Drillet, G.B. Brassington, M. Benkiran, E.P. Chassignet, J.A. Cummings, M. Drevillon, H. Etienne, O. Le Galloudec, E.J. Metzger, and others. 2009. Global high resolution analyses and forecasts at the mesoscale. Pp. 95–111 in *Proceedings Final GODAE Symposium*, November 12–15, 2008, Nice, France.
- Hurlburt, H.E., D.N. Fox, and E.J. Metzger. 1990. Statistical inference of weakly correlated subthermocline fields from satellite altimeter data. *Journal of Geophysical Research* 95(C7):11,375–11,409.
- Hurlburt, H.E., E.J. Metzger, P.J. Hogan, C.E. Tilburg, and J.F. Shriver. 2008b. Steering of upper ocean currents and fronts by the topographically constrained abyssal circulation. *Dynamics of Atmospheres and Oceans* 45:102–134.
- Johns, W.E., T.J. Shay, J.M. Bane, and D.R. Watts. 1995. Gulf Stream structure, transport, and recirculation near  $68^\circ\text{W}$ . *Journal of Geophysical Research* 100(C1):817–838.
- Kanamitsu, M., W. Ebisuzaki, J. Woollen, S.-K. Yang, J.J. Hnilo, M. Fiorino, and G.L. Potter. 2002. NCEP-DOE AMIP-II reanalysis (R-2). *Bulletin of the American Meteorological Society* 83:1,631–1,643.
- Kara, A.B., and H.E. Hurlburt. 2006. Daily interannual simulations of SST and MLD using atmospherically-forced OGCMs: Model evaluation in comparison to buoy time series. *Journal of Marine Systems* 62:95–119.
- Lumpkin, R., and M. Pazos. 2007. Measuring surface currents with SVP drifters: The instrument, its data, and some recent results. Pp. 39–67 in *Lagrangian Analysis and Prediction of Coastal and Ocean Dynamics*. A. Griffa, A.D. Kirwan, A.J. Mariano, T. Özgökmen, and T. Rossby, eds, Cambridge University Press, New York.
- Madec, G. 2008. *NEMO Ocean Engine*. Report 27, ISSN No. 1288-1619. Institut Pierre-Simon Laplace (IPSL), France, 197 pp.
- National Oceanic and Atmospheric Administration, Office of Oceanic and Atmospheric Research Climate Program Office, Climate Observation Division. 2008. *Program Plan for Building a Sustained Ocean Observing System for Climate*. Available online at: [http://www.oco.noaa.gov/docs/programplan\\_current.doc](http://www.oco.noaa.gov/docs/programplan_current.doc) (accessed December 2008).
- Oh, I.S., V. Zhurbas, and W.S. Park. 2000. Estimating horizontal diffusivity in the East Sea (Sea of Japan) and the northwest Pacific from satellite-tracked drifter data. *Journal of Geophysical Research* 105(C3):6,483–6,492.
- Oke, P.R., G.B. Brassington, D.A. Griffin, and A. Schiller. 2008. The Bluelink ocean data assimilation system (BODAS). *Ocean Modelling* 21:46–70.
- Pickart, R.S., and D.R. Watts. 1990. Deep Western Boundary Current variability at Cape Hatteras. *Journal of Marine Research* 48:765–791.
- Ridgeway, K.R., and J.R. Dunn. 2003. Mesoscale structure of the mean East Australian Current system and its relationship to topography. *Progress in Oceanography* 56:190–222.
- Roemmich, D., and the Argo Steering Team. 2009. Argo: The challenge of continuing 10 years of progress. *Oceanography* 22(3):46–55.
- Rosmond, T.E., J. Teixeira, M. Peng, T.F. Hogan, and R. Pauley. 2002. Navy Operational Global Atmospheric Prediction System (NOGAPS): Forcing for ocean models. *Oceanography* 15(1):99–108.
- Schiller, A., P.R. Oke, G.B. Brassington, M. Entel, R. Fiedler, D.A. Griffin, J. Mansbridge. 2008. Eddy-resolving ocean circulation in the Asian-Australian region inferred from an ocean reanalysis effort. *Progress in Oceanography* 76:334–365.
- Shriver, J.F., H.E. Hurlburt, O.M. Smedstad, A.J. Wallcraft, and R.C. Rhodes. 2007.  $1/32^\circ$  real-time global ocean prediction and value-added over  $1/16^\circ$  resolution. *Journal of Marine Systems* 65:3–26.
- Tsujino, H., N. Usui, and H. Nakano. 2006. Dynamics of Kuroshio path variations in a high-resolution general circulation model. *Journal of Geophysical Research* 111, C11001, doi:10.1029/2005JC003118.
- Usui, N., H. Tsujino, and Y. Fujii. 2006. Short-range prediction experiments of the Kuroshio path variabilities south of Japan. *Ocean Dynamics* 56:607–623.
- Usui, N., H. Tsujino, Y. Fujii, and M. Kamachi. 2008a. Generation of a trigger meander for the 2004 Kuroshio large meander. *Journal of Geophysical Research* 113, C01012, doi:10.1029/2007JC004266.
- Usui, N., H. Tsujino, H. Nakano, and Y. Fujii. 2008b. Formation process of the Kuroshio large meander in 2004. *Journal of Geophysical Research* 113, C08047, doi:10.1029/2007JC004675.